A versatile approach to strengthen polymer-based biomedical materials with cellulose nanocrystals

Dr. M. Silva[1], Dr. R. Costa[1], Dr. T. Ferreira[1], Dr. P. Almeida[1]*

[1] Department of Public Health and Epidemiology, University of Minho, Braga, Portugal

Abstract. Cellulose nanocrystals (CNCs) are widely studied as reinforcing fillers for polymers. In many cases the mechanical properties of polymer/CNC nanocomposites do not match the theoretical predictions, arguably on account of CNC aggregation. This problem can be mitigated through the addition of a small amount of a judiciously selected polymeric dispersant that also serves as a binder among the CNCs. We show that the addition of 1-5% w/w poly(vinyl alcohol) (PVA) has a very significant impact on the mechanical properties of poly(ethylene oxide-*co*-epichlorohydrin)/CNC nanocomposites. Remarkable improvements of the stiffness and strength were observed at a PVA content as low as 1% w/w, and the extent of reinforcement increased up to a PVA content of 5% w/w, where Young's modulus, storage modulus, and strength increased by up to 5-fold vis à vis the PVA-free nanocomposites. Similar effects were observed for CNC nanocomposites made with polyurethane or poly(methyl acrylate) matrices, demonstrating that the approach is broadly exploitable. Laser scanning microscopy based resonance energy transfer experiments that involved nanocomposites made with CNCs and PVA that had been labelled with rhodamine and fluorescein, respectively, confirmed that the enhanced mechanical properties of the three-component nanocomposites are indeed related to an improved dispersion of the CNCs.

Introduction

Cellulose nanocrystals (CNCs) are rod-shaped, highly crystalline nanoparticles that can be isolated via acid hydrolysis from many plants and certain animal tissues.[1-5] Their high aspect ratio (between 10 and 100)[6] and stiffness (on-axis tensile modulus of 105 to 143 GPa)[7-8] make them an excellent reinforcing component for polymers.[9-11] The mechanism through which CNCs reinforce a soft polymer matrix is in many cases well described by a percolation model, which defines a critical filler content, above which the stress-transfer process is enabled by a percolating CNC network.[12-13] The largest variation of properties as a function of filler content is usually observed around the onset of percolation. CNCs with high aspect ratio A, such as those isolated from tunicates (A ~73),[14] form percolating networks at low filler concentrations and the derived nanocomposites are typically highly homogeneous.[11] Low-aspect ratio CNCs, such as common CNC types isolated from soft wood pulp (A ~23)[5] or cotton (A ~11)[15-16] must be added in higher concentration to reach the percolation threshold. As a result, the achievable reinforcement is often limited, because the CNCs start to aggregate already at lower concentrations. While the advantages of using CNCs with high aspect ratio are clear, they are commonly isolated from sources that are not viable for technological exploitation, for example tunicates,[16-17] whereas low-aspect-ratio CNCs extracted from soft-pulp wood are now commercially available.[18-19]

The chemical modification of CNCs with small molecules or polymeric grafts has been extensively used to enhance the dispersion of CNCs in a variety of polymers.[20-22] This strategy takes advantage of the reactivity of the hydroxyl groups that are abundant on the surface of these nanoparticles, and has proved very successful to render CNCs compatible with both polar and nonpolar polymer matrices.[23-26] However, this methodology is generally not easy to scale up and the approach requires different modifications, depending on the matrix polymer targeted.

Furthermore, the reinforcement is often lower than expected, arguably because the strength of the interactions between the (modified) CNCs and possibly between CNCs and the matrix is reduced.[27] A more practical way to prevent CNC aggregation in nanocomposites involves the addition of a polymeric additive or "surfactant", which can act as a competitive binder and disrupts CNC-CNC interactions.[28] This strategy was explored by Oksman and coworkers, who investigated the effect of adding large amounts of poly(vinyl alcohol) (PVA, 30% w/w) to poly(lactic acid)/CNC (PLA/CNC) nanocomposites in which strong CNC aggregation was observed, even though the CNC content was low (3.7% w/w).[29-30] The analysis of the resulting materials revealed only a modest improvement of the mechanical properties and macrophase segregation of the PLA and PVA phases, leading to the conclusion that the CNCs were primarily located in the PVA phase. Another polymer capable of interacting with CNCs through hydrogen bonds is poly(ethylene glycol) (PEG). Wolcott and coworkers sought to melt-process poly(3-hydroxybutyrate-*co*-3-hydroxyvalerate)/CNC nanocomposites (PHBV/CNC) utilizing a CNC powder that had been combined with low-molecular-weight PEG; however, CNC agglomeration was observed during freeze-drying. As a result, the melt-processed PHBV/CNC composites exhibited decreased mechanical strength. The amphiphilic properties of high molecular poly(ethylene oxide) (PEO) were later exploited by Dufresne *et al.* to improve the dispersion of CNCs in low-density polyethylene (LDPE).[31] While neat LDPE/CNC composites were inhomogeneous and blackened during extrusion as a result of CNC degradation, the adsorption of PEO on the CNCs' surfaces prior to melt-processing improved their dispersion in the LDPE matrix and limited thermal decomposition. The mechanical properties of these materials were, however, not improved as expected,[32] suggesting that the PEO improved the filler dispersion, but at the same time reduces the filler-filler interactions involved in the stress-transfer. When a poly(ethylene oxide)-*b*-poly(propylene oxide)-*b*-poly(ethylene oxide) triblock copolymer (12.6 kg/mol) was used to modify the surface of CNCs, the rubbery modulus (25 °C) of nanocomposites made with an LDPE matrix increased from ca. 100 MPa (neat LDPE) to ca. 500 MPa.[33] Interestingly, the extent of reinforcement was practically the same for all CNC loadings investigated (1 to 10% w/w). Magniez and coworkers adsorbed poly(ethylene glycol)-*co*-polyethylene (PEG-*co*-PE) on the surface of cellulose microfibrils to improve their compatibility with linear low-density polyethylene (LLDPE).[34] The nanocomposites thus made were homogeneous even at the highest CNC content studied (ca. 23% w/w). PEG-*co*-PE-CNCs were also found to improve the tensile modulus of LLDPE while mitigating the loss of yield strength, and to increase the room-temperature modulus from ca. 200 MPa to ca. 700 MPa (for a 10% w/w CNC content). The PEG-*co*-PE content on the other hand was found to have little influence on the mechanical properties.[31-32, 35]

Thus, a growing body of work supports the conclusion that hydrogen bonding and amphiphilic polymer additives can serve to compatibilize CNCs with a polymer matrix, but the influence on the mechanical reinforcement is typically moderate, and solutions must often be tailored to a specific system. We report here the addition of a small amount of a judiciously selected polymeric additive designed to act as a dispersant and to simultaneously contribute to the stress-transfer. In a systematic study, we employed poly(ethylene oxide-*co*-epichlorohydrin) (EO-EPI) as polymeric matrix, low-aspect ratio CNCs isolated from cotton, and *a small amount of* poly(vinyl alcohol) (PVA) as additive (**Figure 1**).[36-37] Previous work in our group has shown that EO-EPI provides an ideal framework to monitor CNC-induced reinforcement on account of its low modulus and solubility in dimethylformamide, which is also a good dispersing agent for CNCs.[38-41] Interestingly, the reinforcement achieved with high-aspect-ratio CNCs was much higher than

that realized with low-aspect-ratio CNCs,[42-43] which points to CNC aggregation in the latter case.[44] We surmised that the addition of PVA to composites of CNCs and EO-EPI would (i) improve the CNC dispersion, as both the PVA and the CNCs offer many hydroxyl groups that are able to establish hydrogen bonds, and (ii) possibly also act as a binder, enhancing CNC-CNC stress-transfer on account of hydrogen bonding. Indeed, remarkable improvements of the stiffness and strength were observed at a PVA content of 1-5% w/w. Similar effects were observed for CNC nanocomposites made with polyurethane or poly(methyl acrylate) matrices, demonstrating that the approach is broadly exploitable. We employed laser scanning microscopy to analyze nanocomposites made with components that had been labelled with fluorescent dyes and the results confirm that the reason for the enhanced mechanical properties of the three-component nanocomposites are indeed related to an improved dispersion of the CNCs.

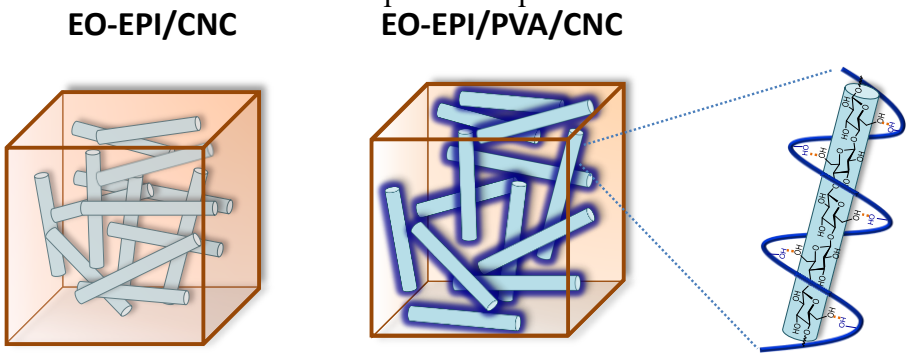

Figure 1. Schematic representation of the proposed mechanism for the enhancement of the mechanical properties of EO-EPI/CNC nanocomposites upon addition of PVA. Through hydrogen bonding, PVA leads to better dispersion of CNCs and supports the formation of a hydrogen-bonded percolating network within the EO-EPI matrix.

Experimental Section

Materials. EO-EPI with a co-monomer ratio of 1 : 1 and a density of 1.39 g/cm^3 was purchased under the tradename epichlomer from Daiso Co., Ltd., Japan. TEXIN 285, a thermoplastic polyurethane (PU) based on poly(tetramethylene glycol), butanediol, and 4,4'-methylenebis(phenyl isocyanate) with a Shore A hardness of approximately 85, was supplied from Bayer Material Science. Poly(methyl acrylate) (PMA) with a molecular weight of 129,000 g/mol was prepared as previously reported.[37] Polyvinyl alcohol (PVA) with a molecular weight of 85,000 – 124,000 g/mol (99% hydrolyzed), fluorescein 5(6)-isothiocyanate (FITC), rhodamine B isothiocyanate (RBITC), dry dimethylformamide (DMF), dimethyl sulfoxide (DMSO) solvent grade and sulfuric acid were purchased from Sigma-Aldrich. Solvent grade methanol was purchased from Honeywell Chemicals. All chemicals were used without further purification. Cotton CNCs, with an average length of 305 ± 80 nm, an average diameter of 27 ± 5, and an average aspect ratio of 11 ± 2, were extracted from Whatman no.1 filter paper by sulfuric acid hydrolysis following our earlier protocol.[43] The aqueous CNCs dispersion was dried by lyophilization using a VirTis BenchTop 2K XL lyophilizer with a condenser temperature of -78 °C.

Miscibility study of PVA in EO-EPI. EO-EPI and PVA (0, 5, 10, 15 or 20% w/w) were dissolved in DMSO (50 mg of EO-EPI per mL) and the mixture was stirred at 70 °C for 10 min. The EO-EPI/PVA solutions were then cast into a round Teflon® Petri-dish with a diameter of 10 cm and dried at 70 °C for 72 h. The dried film of EO-EPI and 5% w/w PVA was further compression-molded in a Carver® press between Teflon® sheets at 70 °C for 5 min with 1500 psi

pressure and this sample was used to further probe the miscibility of EO-EPI and PVA by differential scanning calorimetry.

Preparation of EO-EPI/CNC Nanocomposites. EO-EPI/CNC nanocomposites containing 10% w/w of CNCs and different PVA contents (1-5% w/w) were prepared by solution-casting from DMSO. The dried CNCs were first dispersed in DMSO (10 mg/mL) by stirring for 1 h at room temperature and subsequent sonication in a Sonoswiss SW3H ultrasonic bath for 4 h. The CNC dispersion was then added to a hot (70 °C) solution of EO-EPI in DMSO (50 mg/mL) which had been stirred at 70 °C for 24 h. Subsequently, a PVA solution in DMSO (50 mg/mL) was added at 70°C; the volume was controlled to achieve the desired PVA concentration in the nanocomposite (1, 2, 3, or 5% w/w). For instance, the nanocomposite containing 10% w/w CNCs and 5% w/w PVA was prepared by adding 10 mL of the CNC stock dispersion and 0.9 mL of the PVA solution to 17.1 mL of the EO-EPI solution. The mixture was further stirred at 70 °C for 10 min and subsequently sonicated at room temperature for 30 min before casting it into a round Teflon® Petri-dish with a diameter of 10 cm. The solvent was evaporated in an oven at 70 °C for 72 h and films were subsequently dried under vacuum at 70 °C for 48 h. Finally, the dried films were compression-molded in a Carver® press between Teflon® sheets at 70 °C for 5 min with 1500 psi pressure using spacers to adjust the film thickness to 105 ± 5 µm. Other compositions of EO-EPI/CNC nanocomposites with varying amounts of CNCs (1%, 2.5%, 5%, 6%, 7%, 9%, 15% and 20% w/w) were prepared following the same protocol. Once compression-molded, the samples were stored in a desiccator (containing drierite) at ambient temperature until the mechanical tests were performed to minimize moisture absorption.

Preparation of PU/CNC and PMA/CNC nanocomposites. Following the same protocol as EO-EPI/CNC nanocomposite preparation, PU or PMA were first dissolved in DMSO (50 mg /mL) and stirred overnight. The CNC dispersion in DMSO (10 mg/mL), which was previously sonicated for 4 h, and the PVA solution in DMSO (50 mg/mL) were then added to the polymer solution to obtain the nanocomposites of 10% w/w CNC with and without 5% w/w PVA. The mixture was stirred at 70 °C for 10 min and subsequently sonicated at room temperature for 30 min before casting it into a round Teflon® Petri-dish. Films were dried in an oven at 70 °C for 72 h and subsequently dried under vacuum at 70 °C for 48 h. The dried films were then compression-molded in a Carver® press between Teflon® sheets at 70 °C for 5 min with 1500 psi pressure to adjust the film thickness.

Differential Scanning Calorimetry (DSC). DSC analyses were performed using a Mettler-Toledo STAR under N_2 atmosphere. Samples of ~10 mg were heated from -60 °C to 250 °C and cooled back to -60 °C at 10 °C/min. The degree of crystallinity was calculated by integrating all endothermic peaks observed during the first heating and taking PEO as the 100% crystalline reference.[45]

Dynamic Mechanical Analysis (DMA). The mechanical properties of the EO-EPI/CNC and EO-EPI/PVA/CNC nanocomposite films were studied with a dynamic mechanical analyzer (DMA, TA instruments Model Q800) in tensile mode. The tests were conducted a frequency of 1 Hz and a strain amplitude of 15 µm in the temperature range of -70 to 100 °C at a heating rate of 3 °C/min. Rectangular nanocomposite films with a length of ca. 10 mm a width of 5.30 mm and a thickness of ca. 0.10 mm were used. The mechanical data quoted throughout the text and in Table 1 represent average values of 3 – 5 individual measurements (standard deviation is provided).

The stress strain measurements of these materials were performed in the same DMA instrument with a strain rate of 5%/min at 25 °C. For these experiments, the nanocomposite films were cut into dog-bone-shaped samples and the measurements were performed on 3 – 5 individual samples.

Fluorescent Labelling of PVA and CNCs. PVA and CNCs were functionalized with fluorescein and rhodamine, respectively, in order to enable their visualization by laser scanning microscopy (LSM). PVA was labelled with FITC according to a previous published procedure,[46] wherein PVA (1.00 g) and FITC (0.05 g) were dissolved in dry DMSO (8 mL) and stirred at 90 °C for 3 h. Then the reaction mixture was cooled to room temperature, precipitated three times into methanol (from DMSO) to remove all residual unlinked fluorescein, and dried at 60 °C for 24 h. The functionalization of CNCs was also carried out according to a reported procedure.[47] In brief, a dispersion of CNCs (1.0 g) in dry DMF (250 mL) was sonicated for 4 h, before RBITC (10 mg, 0.1 mol equivalent relative to the total number glucose units in the CNCs) and 1 drop of dibutyltindilaurate were added. The mixture was heated to 100 °C and stirred overnight under N_2. The reaction mixture was subsequently allowed to cool to room temperature and centrifuged 10 times; ethanol and water were alternatingly used to remove any remaining rhodamine. The labelled CNCs were dialyzed against deionized water for 5 days and then dried by lyophilization using a VirTis BenchTop 2K XL lyophilizer with a condenser temperature of -78 °C.

Laser Scanning Microscopy (LSM). Samples of the EO-EPI nanocomposite containing 10% w/w rhodamine-labelled CNCs with and without 5% w/w fluorescein-labelled PVA were prepared by solution-casting from DMSO. The rhodamine-labelled CNCs were first dispersed in DMSO (10 mg/mL) by stirring for 1 h and subsequent sonication in a Sonoswiss SW3H ultrasonic bath for 4 h. The CNC dispersion was added to a hot (70 °C) solution of EO-EPI in DMSO (50 mg/mL) which had been stirred at 70 °C for 24 h. Then, a fluorescein-labelled PVA solution in DMSO (50 mg/mL) was added at 70°C; the volume was controlled to achieve 5% w/w PVA in the nanocomposite. The mixture was further stirred at 70 °C for 10 min and subsequently sonicated at room temperature for 30 min before casting it into a glass slide. The solvent was evaporated in an oven at 70 °C for 2 h. The dried films were used without further treatment. The region of interest was selected using a systematic random sampling procedure: the sample was positioned randomly under the light path of the microscope and each image was recorded exactly 300 μm apart. An acceptor photobleaching method[48] was used to monitor the Förster resonance energy transfer (FRET) between the two fluorophores, i.e. fluorescein-labelled PVA and rhodamine-labelled CNCs. The analyses were performed using a laser scanning microscope (Zeiss LSM 710, Carl Zeiss, AG, Germany) under excitation with lasers operating at 488 nm (Ar gas laser) and 561 nm (diode pumped solid state laser). Each FRET recording consisted of 25 cycles, of which the first five cycles were limited to imaging both fluorescence channels. The last 20 cycles started with a 15 s photobleaching (laser attenuation = 50%) step of the rhodamine-labelled CNCs using the 561 nm laser. After each cycle, the fluorescein-labelled PVA was excited at 488 nm (laser attenuation = 2%) and the emission was recorded using the spectrometer allowing metafilter (a dedicated spectrometer allowing bandpass filter design) to collect light between 493 nm and 452 nm. The rhodamine-labelled CNCs were excited at 561 nm (laser attenuation = 2%) and the emission was recorded using the metafilter to collect light between 566 nm and 703 nm. The fluorescence intensities of the fluorescein labelled donors (PVA) before and after the bleaching of the rhodamine-labelled acceptors (CNCs) were used to calculate the FRET efficiency and the separation distance between two fluorophores. To evaluate

the dispersion of CNCs in the EO-EPI polymer matrix in the presence and absence of PVA, EO-EPI nanocomposite films containing 10% w/w rhodamine-labelled CNC with and without 5% w/w PVA were prepared in DMSO using the procedure mentioned above and analyzed by recording the fluorescence of rhodamine-labelled CNCs when excited at 561 nm.

Laser Scanning Micrograph Image Processing. ISOData[49] was used to perform unsupervised automated cluster analysis of the micrographs. The procedure divides the image into two groups (object and background) by taking an initial threshold, and the averages of the pixels at or below the threshold and the pixels above the threshold are computed. The averages of those two values are computed, the threshold is incremented and the process is repeated until the threshold is larger than the composite average. That is, threshold = (average background + average objects)/2. The procedure separates pixels with high intensities (above the threshold dynamically found by the algorithm) and clusters with pixels which had intensities below that threshold. The quantification was done in ImageJ.[50]

Results and Discussion

We first explored the miscibility of PVA and EO-EPI by preparing a series of CNC-free EO-EPI/PVA blends containing 1 to 20% w/w PVA. Films were prepared via solution-casting from DMSO and vacuum drying. While the addition of up to 5% w/w of PVA resulted in samples of homogeneous appearance, macro-phase separation was observed for PVA contents over 10% w/w (Supporting Figure S1a). Thus, only PVA loads between 1% and 5% w/w were used in subsequent experiments to test the effect of PVA on the mechanical properties of cellulose-based nanocomposites. A comparison of the differential scanning calorimetry traces of neat EO-EPI, neat PVA, and a blend of EO-EPI and 5% w/w PVA (Supporting Figure S1ab) shows no evidence for phase separation in the blend. Furthermore, the addition of PVA or CNCs to EO-EPI did not induce a change the host polymer's degree of crystallinity (**Supporting Table S2**).

A first series of EO-EPI/PVA/CNC nanocomposites was prepared in which the CNCs content was kept constant at 10% w/w and the PVA content was varied (0, 1, 3 and 5% w/w). Nanocomposite films were prepared by solution casting and subsequent compression molding. DMSO was used instead of the customary DMF[38-39, 43, 51-52] for the casting step, because of the low solubility of PVA in DMF. The films thus made were transparent (Supporting Figure S2), providing a first indication that the CNCs were well dispersed in the EO-EPI matrix at all compositions. The mechanical properties of the neat EO-EPI and the nanocomposites were studied using dynamic mechanical analysis (DMA) and tensile testing. The DMA data (**Figure 2a, Table 1**) show that the room temperature storage modulus *E'* is increased from ~3 MPa (neat EO-EPI) to 50 MPa upon introduction of 10% w/w CNCs. Remarkably *E'* increased to 106 MPa if in addition to the CNCs 1% w/w PVA was incorporated. Upon further raising the PVA content to 5% w/w, *E'* increased to 206 ± 16 MPa. By contrast, blending the neat EO-EPI with 1-5% w/w of PVA did not cause any significant change of *E*', which rules out any reinforcing effect caused by the PVA alone.

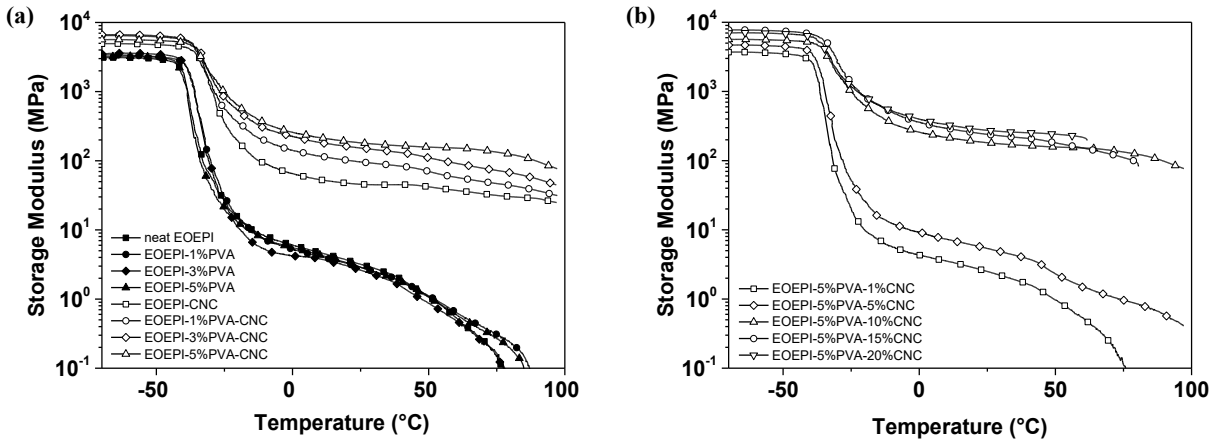

Figure 2. Representative DMA traces of (a) neat EO-EPI, EO-EPI/PVA blends with 1, 3, and 5% w/w PVA (filled symbols) and EO-EPI/PVA/CNC nanocomposites containing 10% w/w CNCs (empty symbols) and ~~0–5%~~1, 3, and 5% w/w PVA; and (b) EO-EPI/PVA/CNC nanocomposites containing 5% w/w PVA and 1, 5, 10, 15, and 20% w/w CNCs.

Given that for EO-EPI with 10% w/w CNCs *E*' increased with the PVA content and that phase separation was observed above a PVA content of 5% w/w (*vide supra*), a second series of nanocomposites was prepared, in which the PVA content was fixed at 5% w/w and the CNC content was varied between 1 and 20% w/w. The DMA traces (**Figure 2b**) show that below and above the glass transition temperature *E'* increases in a nonlinear manner with the CNC content to reach 6.8 GPA (-60 º) and 251 MPa (room temperature) at a CNC content of 20% w/w. A steep increase of *E*' is observed between 5 and 10% w/w CNCs, due to the onset of percolation in this regime (*vide infra*), whereas much less pronounced change of *E*' occurred when the CNC content was further increased.

Table 1. Storage moduli of EO-EPI/PVA blends and EO-EPI/PVA/CNC nanocomposites.[a]

Composition	Storage Modulus, *E'* (MPa)	
	At -60 °C	At 25 °C
Neat EO-EPI	2896 ± 311	2.9 ± 0.4
EO-EPI/1%PVA	3227 ± 110	2.6 ± 0.3
EO-EPI/3%PVA	3210 ± 331	2.3 ± 0.3
EO-EPI/5%PVA	3098 ± 156	2.7 ± 0.2
EO-EPI/10%CNC	5314 ± 353	50 ± 4
EO-EPI/1%PVA/10%CNC	6807 ± 337	106 ± 9

EO-EPI/3%PVA/10%CNC	6663 ± 186	136 ± 18
EO-EPI/5%PVA/10%CNC	5800 ± 231	206 ± 16
EO-EPI/5%PVA/1%CNC	3509 ± 194	2.2 ± 0.3
EO-EPI/5%PVA/5%CNC	4592 ± 53	5.3 ± 0.6
EO-EPI/5%PVA/15%CNC	7691 ± 10	230 ± 13
EO-EPI/5%PVA/20%CNC	6806 ± 378	251 ± 24

[a]Data were acquired from DMA analyses and represent averages of N = 3–5 individual measurement, ± standard deviation.

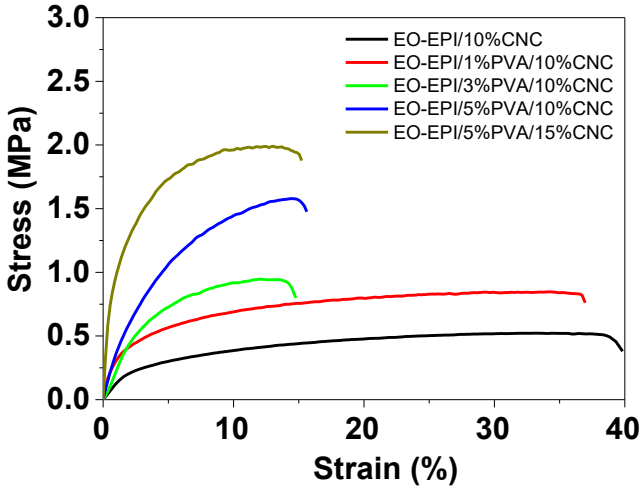

Figure 3. Representative stress-strain curves of EO-EPI/PVA/CNC nanocomposites containing 10 or 15% w/w CNCs and 0-5% w/w PVA. Data were acquired at 25 °C.

Table 2. Tensile properties of EO-EPI/PVA/CNC nanocomposites.[a]

Composition	Young's modulus (MPa)	Tensile strength (MPa)	Elongation at break (%)
EO-EPI/10%CNC	13 ± 4	0.50 ± 0.07	39.9 ± 0.9
EO-EPI/1%PVA/10%CNC	24 ± 1	0.89 ± 0.07	39.2 ± 2.3
EO-EPI/3%PVA/10%CNC	35 ± 6	0.96 ± 0.03	14.7 ± 1.3
EO-EPI/5%PVA/10%CNC	43 ± 9	1.53 ± 0.09	13.7 ± 1.6
EO-EPI/5%PVA/15%CNC	64 ± 9	1.98 ± 0.08	17.1 ± 1.4

[a]Data were acquired from tensile tests at 25ºC and represent averages of N = 3–5 individual measurement, ± standard deviation.

The influence of introducing PVA on the mechanical properties of EO-EPI/CNC nanocomposites was further investigated by tensile tests that were carried out at 25 °C. The stress strain curves confirm the reinforcement of EO-EPI/CNC nanocomposites with PVA and highlight the effect of PVA content on their mechanical properties (**Figure 3**). The Young's moduli mirror the changes observed in *E'*; the composites with a CNC content of 10% w/w display an increase from 13 MPa for the PVA-free EO-EPI/CNC nanocomposite to 24 and 43 MPa for the nanocomposites containing 1 and 5% w/w PVA, respectively (**Table 2**). A further increase to 64 MPa was observed for the composition with 5% PVA and 15% w/w CNCs. A similar trend was observed for the tensile strength, while the elongation at break was reduced from 40% to 14% when the neat EO-EPI/CNC nanocomposite was loaded with 5% w/w PVA. Thus, both the strength and stiffness of the EO-EPI/CNC nanocomposites could be approximately quadrupled upon introduction of a minimal amount (5% w/w) of PVA. This reinforcement is much higher than that observed when PEO was introduced into LDPE/CNC nanocomposites,[32] where the tensile strength increased from ca. 8.5 MPa to ca. 9.0 MPa. Thus, the experimental data support our initial hypothesis that the addition of a small amount of PVA nanocomposites can enhance the mechanical properties of CNC-based nanocomposites considerably.

In order to probe the generality of the approach, we also introduced PVA into CNC nanocomposites made with a thermoplastic polyurethane (PU) and a poly(methyl acrylate) (PMA) matrix. As in the case of the EO-EPI/CNC composites, thin films were made by casting from DMSO followed by compression molding. **Figure 4** shows the DMA traces of the neat PU, PVA-free nanocomposites containing 10% w/w CNCs, and the corresponding nanocomposites made with 5% w/w PVA. Neat PMA could not be analyzed by DMA as it has a T_g of 10 °C and therefore cannot be processed and handled at room temperature. A comparison of the data clearly shows that in both systems *E'* increases substantially upon introduction of PVA, both below and above T_g. For example at room temperature, *E'* of the PU increased from 70 ± 7 MPa to 425 ± 20 MPa upon introduction of CNCs, and rose further to 1025 ± 40 MPa, when the PVA was included. The *E*' values of the PMA-based nanocomposites without (1425 ± 15 MPa) and with (1745 ± 25 MPa) PVA show a similarly large difference. Thus, all data collected support the conclusion that the effect is general and broadly exploitable. The fact that PVA addition has a similar effect in different types of matrix polymers is a first indication that the PVA primarily interacts with the CNCs and that the observed increase of the reinforcement is related to improved dispersion of the nanofillers (*vide infra*).

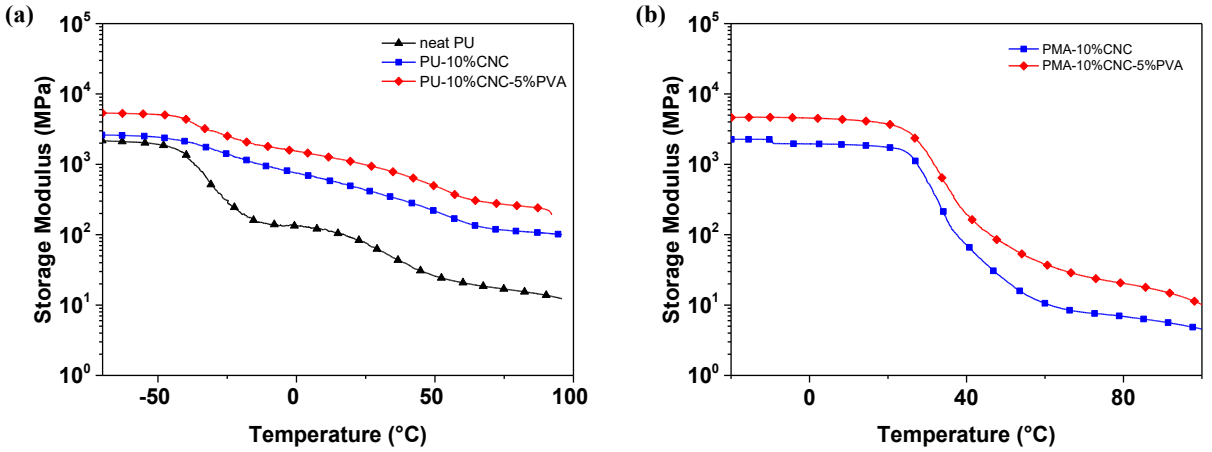

Figure 4. Representative DMA traces of (a) neat PU and PU/CNC nanocomposites containing 10% w/w of CNCs and optionally 5% w/w PVA; and (b) PMA/CNC nanocomposite containing 10% w/w of CNCs with and optionally 5% w/w PVA.

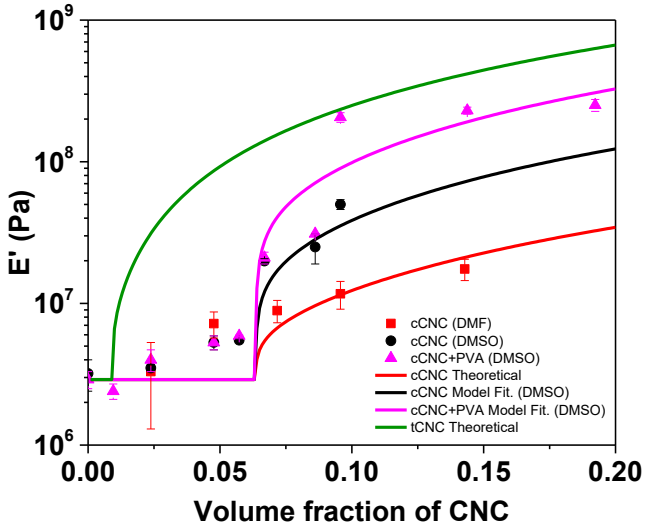

Figure 5. Experimental data (symbols) and values predicted by a percolation model (lines, see text for details) of the tensile storage modulus (*E'*) of EO-EPI/CNC nanocomposites made with CNCs isolated from cotton. Shown are values for PVA-free nanocomposites that were casted from DMF (red line, squares, taken from Ref. [44]) or DMSO (black line, circles), and 5% w/w PVA containing nanocomposites casted from DMSO (pink line, triangles). In addition to these data/fits a corresponding fit of the *E'* values of nanocomposites made with CNCs isolated from tunicates is shown for reference purposes (green line, fit from Ref. [44]).

To better understand the mechanism through which PVA reinforces the CNC nanocomposites investigated here, we analyzed the experimental *E'* values of PVA-free EO-EPI/CNC nanocomposites and the 5% w/w PVA containing EO-EPI/PVA/CNC nanocomposites cast from DMSO (which were all made with CNCs isolated from cotton) in the framework of a percolation model that is commonly used to describe the stiffness of nanocomposites with high-aspect ratio nanofillers (**Figure 5, Supporting Table S1**).[42-43, 53] The parameters used to fit the experimental data against the model include the experimentally determined CNC aspect ratio *A* of 11, the

measured matrix tensile storage modulus of 2.9 MPa, and a percolation exponent of 0.4, whereas the stiffness of the reinforcing CNC phase was used as a fit parameter (**SI Supplementary discussion**). As benchmarks, we also show data and fit acquired for the PVA-free EO-EPI/CNC nanocomposites made with CNCs cast from DMF (the most commonly used solvent to process CNCs, *the data points and fit were taken from Ref. [44]*) and the percolation model's fit of the *E'* values of PVA-free EO-EPI/CNC nanocomposites made with high-aspect ratio (A = 76) CNCs isolated from tunicates (for experimental data and fit parameters see Ref. [44], **SI Supplementary discussion**). The data paint an interesting picture. Up to the onset of percolation at a volume fraction of ca. 6% v/v, the experimentally determined *E'* values of the three series of EO-EPI/CNC nanocomposites follow the same trace (note that the model used neglects any reinforcement in this regime). At this point, a steep, step-wise increase in *E'* is seen for the PVA-free and PVA-containing composites processed from DMSO. By contrast, *E'* of the material cast from DMF increases more gradually and the curve asymptotes towards a much lower level of reinforcement than observed for the other series. Interestingly the *E*' values of the two series cast from DMSO also diverge as the CNC content is increased beyond 8% v/v, and a much higher reinforcement level is observed for the PVA-containing materials. This extent of reinforcement seems to be unprecedented for CNCs isolated from cotton, and approaches that observed for high-aspect ratio CNCs isolated from tunicates. We speculate that the data reflect the extent/quality of CNC dispersion in the respective compositions. At low filler content (< 6% v/v), the CNCs appear to be well dispersed in all three series, and similar reinforcement levels are reached. In the series processed from DMF, one of the most widely used solvents for the processing of CNC composites, aggregation of CNCs appears to take overhand before a percolating network is formed, suggesting that processing conditions may not be as good as previously assumed, at least in the matrices investigated here. When processed from DMSO, the CNCs appear to be well-dispersed up to the onset of percolation, but at higher CNC content the aggregation of CNCs appears to limit full network formation. The best dispersion seems to be possible by employing PVA, and consequently *E*' continues to increase well past the onset of percolation, although also in this case, *E*' levels off at a CNC content of 10% v/v, suggesting aggregation at higher filler volumes. Overall, the experimental data adjust reasonably well to the values predicted by the percolation model. The differences observed are the expected between idealized and experimental data, which arise from the CNC particle size distribution, the processing method or the presence of particle aggregates.

In order to support this explanation and gain a better insight in the role of PVA in the dispersion of CNCs, we prepared EO-EPI/CNC and EO-EPI/PVA/CNC nanocomposites containing 10% w/w of rhodamine-labelled CNCs and 5% w/w of PVA for the observation of the distribution of CNCs within the polymer matrix analysis by laser scanning microscopy (LSM). The rhodamine-labelled CNCs were prepared according to a reported procedure[47] and UV-vis absorption spectra revealed a degree of functionalization of 3.0 mmol/kg (Supporting Figure S3). EO-EPI/CNC nanocomposite films containing 10% w/w of the rhodamine-labelled CNCs and optionally 5% w/w PVA were produced by solution-casting from DMSO. The LSM micrographs of the PVA-free nanocomposite clearly show the formation of large clusters or aggregates of CNCs with characteristic dimensions in the range of tens of micrometers (**Figure 6a**). Smaller CNC aggregates were observed when the nanocomposite contained PVA (**Figure 6b**), with aggregate sizes between 1 μm and 10 μm. Pixel classifications by ISOData (Supporting Figure S4) allowed to assign pixels with intensities above the threshold (PIAT) set by the algorithm, coinciding with the large aggregates, and pixels belonging to pixels with intensities below the threshold (PIBT),

coinciding with the apparently diffuse background. Average intensities for both groups were retrieved and compared for the different samples.[49] Although the overall fluorescence signal originating from rhodamine-labelled CNCs did not decrease upon the addition of 5% w/w PVA (Supporting Figure S5), a significant decrease of the contribution of PIAT from 70% to 42% was observed, whereas the PIBT contribution rose accordingly (**Figure 6c**): These results unequivocally confirm the role of PVA in reducing the formation of large CNC aggregates and thus the anticipated connection between CNCs dispersion and mechanical reinforcement.

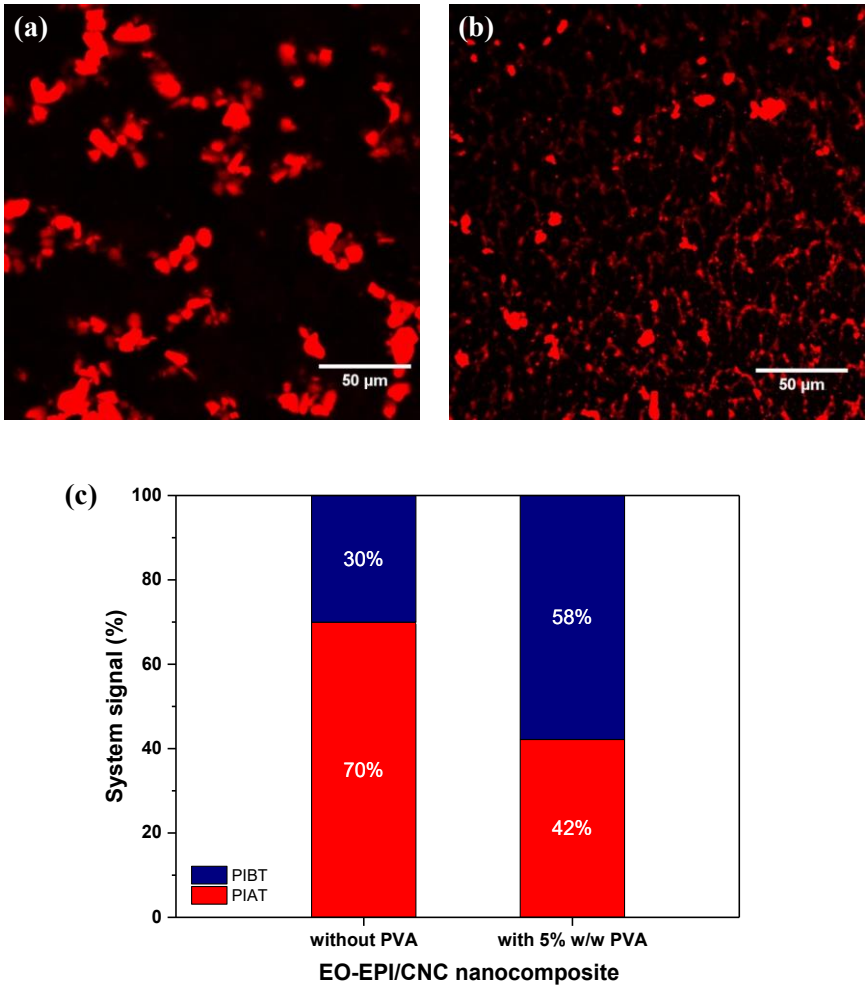

Figure 6. Representative laser scanning microscopy (LSM) images of EO-EPI/CNC nanocomposite films containing 10% w/w of the rhodamine-labelled CNCs. The samples were solution-cast from DMSO and were either PVA free (a) or contained 5% w/w PVA (b). The bar graph (c) displays the fraction of high intensity pixels (PIAT), typically associated with large CNC aggregates and low intensity pixels (PIBT), associated with dispersed CNCs (see text for details). Data is based on n=14 randomly chosen datasets.

In order to act as a dispersant for the CNCs, the PVA must be localized on the CNCs' surface, where it can mitigate CNC-CNC and perhaps also CNC-matrix interactions. In order to verify this, we studied the interactions between the CNCs and PVA in the nanocomposites, by recording the Förster resonance energy transfer (FRET) signal between two fluorophores.[54] Unlike the

FRET molecules used in a previous study of the interface between nanofibrillated cellulose and a matrix polymer[55], both chromophore types were covalently attached to the components thought to form the interface, i.e., the CNCs and the PVA. With the rhodamine-labelled CNCs in hand (*vide supra*) and with reference to many studies that have used the fluorescein / rhodamine FRET pair to probe molecular interactions in biomolecules,[56-58] we functionalized PVA with fluorescein, using a recently reported procedure (degree of functionalization = 6.8 mmol/kg, Supporting Figure S6).[46] EO-EPI/PVA/CNC nanocomposite films containing 10% w/w rhodamine-labelled CNCs and 5% w/w fluorescein-labelled PVA were prepared by casting from DMSO. The specific FRET technique employed relied on abolishing the acceptor fluorescence (rhodamine) by a series of photobleaching cycles (bleaching wavelength = 561 nm). If FRET was at play, the bleaching of the acceptor must be accompanied by an increase of the donor fluorescence (fluorescein-labelled PVA) since its energy can no longer be funneled to the acceptor. This method permits the quantification of the extent of energy transfer efficiency or relative efficiency (E_{rel}) and the average distance between the two types of chromophores involved. Immediately after each photobleaching cycle of the acceptor (rhodamine-labelled CNC), the fluorescence signal of the nanocomposite, both rhodamine-labelled CNC and fluorescein-labelled PVA, was recorded. False color LSM images recorded immediately before and after the photobleaching cycles of the acceptor (rhodamine-labelled CNC) show the emission intensity of the donor (fluorescein-labelled PVA, green in **Figure 7a,c**) and the acceptor (rhodamine-labelled CNCs, red in **Figure 7b,d**). The images show similar morphological features as seen in **Figure 6**, i.e., a few aggregates with a diameter between 1 µm and 10 µm that are scattered within a diffuse background in which the CNCs are presumably well dispersed. Before the photobleaching cycles (**Figure 7a,b**), the signals of the donor and acceptor mirror each other, suggesting co-localization of CNCs and PVA both in in regions with high fluorescence intensity and low fluorescence intensity. After the photobleaching cycles (**Figure 7 c,d**) the acceptor signal (rhodamine-labelled CNCs, red) is abolished while the intensity of the donor signal (fluorescein-labelled PVA, green) is strongly increased. This observation reveals unequivocally that in the pristine samples FRET occurs. **Figure 8a** shows the change of fluorescence intensities after each photobleaching step, revealing the dynamics of the procedure. The first five cycles were programmed to perform no photobleaching and the emission intensity of both donor and emitter remains stable. The region of interest was subseqently exposed to 20 cycles of bleaching using the acceptor exciting laser (561 nm laser, attenuation = 50%) for 15 seconds per cycle. After each cycle, an image of both acceptor (rhodamine-labelled CNCs, excited at 561 nm excitation) and donor (fluorescein-labelled PVA, excited 488 nm excitation) was recorded at a much lower laser attenuation (2%), the same intensity that was used to image the nanocomposite in **Figure 6**. On account of the photobleaching, the fluorescence intensity of the rhodamine acceptor drops with each additional cycle, and a corresponding increase of the fluorescein donor intensity is seen. This behaviour clearly confirms a functional FRET pair, confirming that CNCs and PVA are within FRET distance (< 10 nm) in the polymer matrix. By applying the ISOData again, the image can be classified in groups of PIAT found by algorithm and clusters with PIBT. A functional FRET was found in both groups (**Figure 8a**). The relative FRET efficiency E_{rel} can be calculated using Eq. (1):

$$E_{rel} = 100 \cdot \frac{I_{pre} - I_{post}}{I_{post}} \quad (1)$$

in which I relates to the intensity of the donor and I_{pre} is the average fluorescence intensity before photobleaching (during the first 5 cycles) and I_{post} is the average fluorescence intensity after photobleaching (during the last 5 cycles). The slight decrease in average donor intensities after 20

or so cycles can most probably be attributed to imaging-induced bleaching effects. The distance (r) between donor and acceptor was then calculated using Eq. (2):

$$r = R_0 \sqrt[6]{\left(\frac{1}{E_{rel}}\right) - 1} \quad (2)$$

where R_0 is the Förster distance of the fluorescein/rhodamine FRET pair (55Å[59]), i.e. the distance at which the energy transfer efficiency is 50%. **Figure 8b** shows the average distance between rhodamine-labelled CNC and fluorescein-labelled PVA, which was found to in the same range for both groups: 46.9 Å in the group of PIAT and 48.1 Å in the group of PIBT. These data imply that PVA and CNCs are located all over the nanocomposite network, at a distance that supports their interaction via hydrogen bonding.

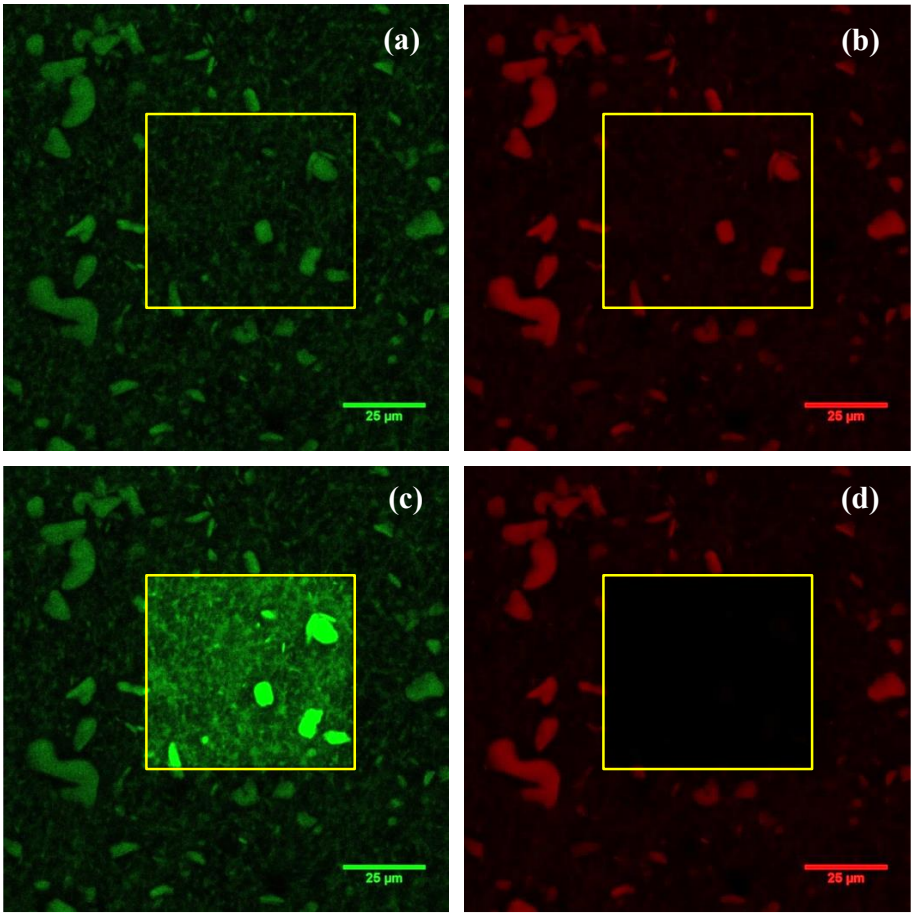

Figure 7. Laser scanning microscopy images visualizing the emission of EO-EPI/PVA/CNC nanocomposites containing 10% w/w rhodamine-labelled CNCs (acceptor, red) and 5% w/w fluorescein-labelled PVA (donor, green) before (a,b) and after photobleaching the acceptor in the area marked by yellow squares (c,d). Shown are false colour images reflecting the emission intensity from (a,c) the donor-labelled PVA (excited at 488 nm and recorded through a 493 - 542 nm metafilter) and (b,d) the acceptor-labelled CNCs (excited at 561 nm and recorded through a 566 - 703 nm metafilter).

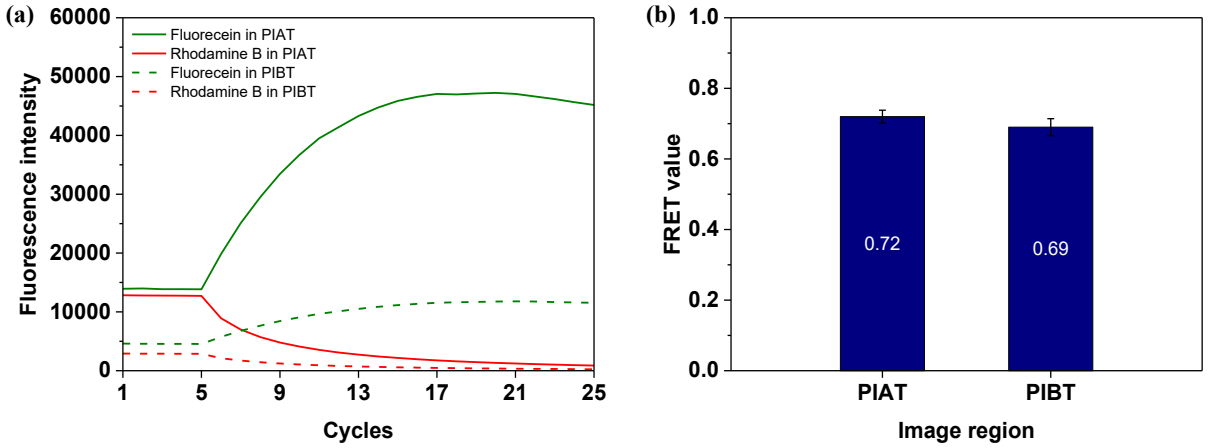

Figure 8. (a) Graph displaying the fluorescence intensities of 10% w/w rhodamine-labelled CNCs (acceptor, red line) and 5% w/w fluorescein-labelled PVA (donor, green line) in EO-EPI/PVA/CNC nanocomposite. Data were acquired by analyzing laser scanning microscopy images of the nanocomposite after acceptor photobleaching. Photobleaching was started after five cycles and the acceptor was increasingly bleached. (b) Bar graph showing the FRET efficiency calculated from the fluorescence intensities in different regions of the composite. For the analysis, laser scanning microscopy images were partitioned into high intensity pixels (pixel intensity above threshold; PIAT), typically associated with large CNC aggregates and low intensity pixels (pixel intensity below threshold; PIBT), associated with dispersed CNCs (see text for details).

Conclusions

In summary, we have shown that the incorporation of small amounts of PVA (1–5% w/w) into EO-EPI/CNC nanocomposites leads to a significant enhancement of the mechanical properties. Above the percolation threshold, both the stiffness and tensile strength were quadrupled upon introduction of only 5% w/w PVA and, most importantly, a similar effect was observed when PVA was incorporated to polyurethane/CNC and poly(methyl acrylate)/CNC nanocomposites, which suggests that this approach may be applied to reinforce a wide range of polymeric matrices. Light scanning microscopy was used to gain unprecedented insight in the *in matrix* morphology of and interactions between CNCs and hydrogen bonding polymeric additives. The analyses showed that CNCs are more evenly distributed within the polymer matrix in the presence of PVA, and that PVA and CNCs are co-localized within hydrogen bonding distance, which supports the hypothesis that PVA enhances stress transfer by improving CNCs dispersion. This visual proof of the effect of PVA on CNC aggregation suggests that traditional CNC-based nanocomposites, and by extrapolation other high aspect ratio nanofiller-based nanocomposites, may contain an overlooked and relatively high fraction of filler aggregates even if the desired mechanical reinforcement is achieved.

Acknowledgments

The authors gratefully acknowledge financial support from the Swiss National Science Foundation (Ambizione grant to LME) and the Adolphe Merkle Foundation. We thank Michela

di Giannantonio for kindly providing the PMA. WM thanks the Swiss Confederation for a doctoral scholarship.

Supporting Information

DSC traces of PVA, EO-EPI, an EO-EPI/PVA blend, and an EO-EPI/CNC nanocomposite. Pictures of EO-EPI/PVA and EO-EPI/PVA/CNC nanocomposite films and details of fitting of mechanical properties with percolation model. Determination of the dye concentration on PVA and CNCs by UV-Vis spectroscopy. LSM image ISOData processing and analysis.

Note

The authors declare no competing financial interest.

References

1. Beck-Candanedo, S.; Roman, M.; Gray, D. G. Effect of Reaction Conditions on the Properties and Behavior of Wood Cellulose Nanocrystal Suspensions. *Biomacromolecules* **2005,** *6*, 1048-1054.

2. George, J.; Ramana, K. V.; Bawa, A. S.; Siddaramaiah Bacterial Cellulose Nanocrystals Exhibiting High Thermal Stability and Their Polymer Nanocomposites. *International Journal of Biological Macromolecules* **2011,** *48*, 50-57.

3. Johar, N.; Ahmad, I.; Dufresne, A. Extraction, Preparation and Characterization of Cellulose Fibres and Nanocrystals from Rice Husk. *Industrial Crops and Products* **2012,** *37*, 93-99.

4. Klemm, D.; Kramer, F.; Moritz, S.; Lindström, T.; Ankerfors, M.; Gray, D.; Dorris, A. Nanocelluloses: A New Family of Nature-Based Materials. *Angewandte Chemie International Edition* **2011,** *50*, 5438-5466.

5. Sacui, I. A.; Nieuwendaal, R. C.; Burnett, D. J.; Stranick, S. J.; Jorfi, M.; Weder, C.; Foster, E. J.; Olsson, R. T.; Gilman, J. W. Comparison of the Properties of Cellulose Nanocrystals and Cellulose Nanofibrils Isolated from Bacteria, Tunicate, and Wood Processed Using Acid, Enzymatic, Mechanical, and Oxidative Methods. *ACS Applied Materials & Interfaces* **2014,** *6*, 6127-6138.

6. Moon, R. J.; Martini, A.; Nairn, J.; Simonsen, J.; Youngblood, J. Cellulose Nanomaterials Review: Structure, Properties and Nanocomposites. *Chemical Society Reviews* **2011,** *40*, 3941-3994.

7. Rusli, R.; Eichhorn, S. J. Determination of the Stiffness of Cellulose Nanowhiskers and the Fiber-Matrix Interface in a Nanocomposite Using Raman Spectroscopy. *Applied Physics Letters* **2008,** *93*, 033111.

8. Šturcová, A.; Davies, G. R.; Eichhorn, S. J. Elastic Modulus and Stress-Transfer Properties of Tunicate Cellulose Whiskers. *Biomacromolecules* **2005,** *6*, 1055-1061.

9. Garcia de Rodriguez, L. N.; Thielemans, W.; Dufresne, A. Sisal Cellulose Whiskers Reinforced Polyvinyl Acetate Nanocomposites. *Cellulose* **2006,** *13*, 261-270.

10. Rueda, L.; Saralegui, A.; Fernández d'Arlas, B.; Zhou, Q.; Berglund, L. A.; Corcuera, M. A.; Mondragon, I.; Eceiza, A. Cellulose Nanocrystals/Polyurethane Nanocomposites. Study from the Viewpoint of Microphase Separated Structure. *Carbohydrate Polymers* **2013,** *92*, 751-757.

11. Sapkota, J.; Jorfi, M.; Weder, C.; Foster, E. J. Reinforcing Poly(Ethylene) with Cellulose Nanocrystals. *Macromolecular Rapid Communications* **2014,** *35*, 1747-1753.

12. Eichhorn, S. J.; Dufresne, A.; Aranguren, M.; Marcovich, N. E.; Capadona, J. R.; Rowan, S. J.; Weder, C.; Thielemans, W.; Roman, M.; Renneckar, S.; Gindl, W.; Veigel, S.; Keckes, J.; Yano, H.; Abe, K.; Nogi, M.; Nakagaito, A. N.; Mangalam, A.; Simonsen, J.; Benight, A. S.; Bismarck, A.; Berglund, L. A.; Peijs, T. Review: Current International Research into Cellulose Nanofibres and Nanocomposites. *Journal of Materials Science* **2009,** *45*, 1-33.

13. Habibi, Y.; Lucia, L. A.; Rojas, O. J. Cellulose Nanocrystals: Chemistry, Self-Assembly, and Applications. *Chemical Reviews* **2010,** *110*, 3479-3500.

14. Mueller, S.; Sapkota, J.; Nicharat, A.; Zimmermann, T.; Tingaut, P.; Weder, C.; Foster, E. J. Influence of the Nanofiber Dimensions on the Properties of Nanocellulose/Poly(Vinyl Alcohol) Aerogels. *Journal of Applied Polymer Science* **2015,** *132*, doi:10.1002/app.41740.

15. Jorfi, M.; Roberts, M. N.; Foster, E. J.; Weder, C. Physiologically Responsive, Mechanically Adaptive Bio-Nanocomposites for Biomedical Applications. *ACS Applied Materials & Interfaces* **2013,** *5*, 1517-1526.

16. Sapkota, J.; Natterodt, J. C.; Shirole, A.; Foster, E. J.; Weder, C. Fabrication and Properties of Polyethylene/Cellulose Nanocrystal Composites. *Macromolecular Materials and Engineering* **2016,** doi:10.1002/mame.201600300.

17. Cudjoe, E.; Hunsen, M.; Xue, Z.; Way, A. E.; Barrios, E.; Olson, R. A.; Hore, M. J. A.; Rowan, S. J. Miscanthus Giganteus: A Commercially Viable Sustainable Source of Cellulose Nanocrystals. *Carbohydrate Polymers* **2017,** *155*, 230-241.

18. *Annual Report 2011-2012: Strategic and Financial Review*; FPInnovations: Canada, **2012**.

19. Ozcan, S.; Tekinalp, H. L.; Love, L. J.; Kunc, V.; Nelson, K. *Low-Cost Nanocellulose-Reinforced High-Temperature Polymer Composites for Additive Manufacturing*; United States, 2016-07-13, **2016**.

20. Natterodt, J. C.; Sapkota, J.; Foster, E. J.; Weder, C. Polymer Nanocomposites with Cellulose Nanocrystals Featuring Adaptive Surface Groups. *Biomacromolecules* **2017**, *18,* 517-525.

21. Goffin, A.-L.; Raquez, J.-M.; Duquesne, E.; Siqueira, G.; Habibi, Y.; Dufresne, A.; Dubois, P. From Interfacial Ring-Opening Polymerization to Melt Processing of Cellulose Nanowhisker-Filled Polylactide-Based Nanocomposites. *Biomacromolecules* **2011,** *12*, 2456-2465.

22. Miao, C.; Hamad, W. Y. Cellulose Reinforced Polymer Composites and Nanocomposites: A Critical Review. *Cellulose* **2013,** *20*, 2221-2262.

23. Freire, C. S. R.; Silvestre, A. J. D.; Neto, C. P.; Gandini, A.; Martin, L.; Mondragon, I. Composites Based on Acylated Cellulose Fibers and Low-Density Polyethylene: Effect of the Fiber Content, Degree of Substitution and Fatty Acid Chain Length on Final Properties. *Composites Science and Technology* **2008,** *68*, 3358-3364.

24. Junior de Menezes, A.; Siqueira, G.; Curvelo, A. A. S.; Dufresne, A. Extrusion and Characterization of Functionalized Cellulose Whiskers Reinforced Polyethylene Nanocomposites. *Polymer* **2009,** *50*, 4552-4563.

25. Raquez, J. M.; Murena, Y.; Goffin, A. L.; Habibi, Y.; Ruelle, B.; DeBuyl, F.; Dubois, P. Surface-Modification of Cellulose Nanowhiskers and Their Use as Nanoreinforcers into Polylactide: A Sustainably-Integrated Approach. *Composites Science and Technology* **2012,** *72*, 544-549.

26. Yu, H.-Y.; Qin, Z.-Y. Surface Grafting of Cellulose Nanocrystals with Poly(3-Hydroxybutyrate-Co-3-Hydroxyvalerate). *Carbohydrate Polymers* **2014,** *101*, 471-478.

27. Gopalan Nair, K.; Dufresne, A.; Gandini, A.; Belgacem, M. N. Crab Shell Chitin Whiskers Reinforced Natural Rubber Nanocomposites. 3. Effect of Chemical Modification of Chitin Whiskers. *Biomacromolecules* **2003,** *4*, 1835-1842.

28. Oksman, K.; Aitomäki, Y.; Mathew, A. P.; Siqueira, G.; Zhou, Q.; Butylina, S.; Tanpichai, S.; Zhou, X.; Hooshmand, S. Review of the Recent Developments in Cellulose Nanocomposite Processing. *Composites Part A: Applied Science and Manufacturing* **2016,** *83*, 2-18.

29. Bondeson, D.; Oksman, K. Polylactic Acid/Cellulose Whisker Nanocomposites Modified by Polyvinyl Alcohol. *Composites Part A: Applied Science and Manufacturing* **2007,** *38*, 2486-2492.

30. Kvien, I.; Oksman, K. Orientation of Cellulose Nanowhiskers in Polyvinyl Alcohol. *Applied Physics A* **2007,** *87*, 641-643.

31. Ben Azouz, K.; Ramires, E. C.; Van den Fonteyne, W.; El Kissi, N.; Dufresne, A. Simple Method for the Melt Extrusion of a Cellulose Nanocrystal Reinforced Hydrophobic Polymer. *ACS Macro Letters* **2012,** *1*, 236-240.

32. Pereda, M.; Kissi, N. E.; Dufresne, A. Extrusion of Polysaccharide Nanocrystal Reinforced Polymer Nanocomposites through Compatibilization with Poly(Ethylene Oxide). *ACS Applied Materials & Interfaces* **2014,** *6*, 9365-9375.

33. Nagalakshmaiah, M.; Pignon, F.; El Kissi, N.; Dufresne, A. Surface Adsorption of Triblock Copolymer (Peo-Ppo-Peo) on Cellulose Nanocrystals and Their Melt Extrusion with Polyethylene. *RSC Advances* **2016,** *6*, 66224-66232.

34. Volk, N.; He, R.; Magniez, K. Enhanced Homogeneity and Interfacial Compatibility in Melt-Extruded Cellulose Nano-Fibers Reinforced Polyethylene Via Surface Adsorption of Poly(Ethylene Glycol)-Block-Poly(Ethylene) Amphiphiles. *European Polymer Journal* **2015,** *72*, 270-281.

35. Arias, A.; Heuzey, M.-C.; Huneault, M. A.; Ausias, G.; Bendahou, A. Enhanced Dispersion of Cellulose Nanocrystals in Melt-Processed Polylactide-Based Nanocomposites. *Cellulose* **2015,** *22*, 483-498.

36. Pereira, A. L. S.; Nascimento, D. M. d.; Souza Filho, M. d. s. M.; Morais, J. P. S.; Vasconcelos, N. F.; Feitosa, J. P. A.; Brígida, A. I. S.; Rosa, M. d. F. Improvement of Polyvinyl Alcohol Properties by Adding Nanocrystalline Cellulose Isolated from Banana Pseudostems. *Carbohydrate Polymers* **2014,** *112*, 165-172.

37. Sonker, A. K.; Tiwari, N.; Nagarale, R. K.; Verma, V. Synergistic Effect of Cellulose Nanowhiskers Reinforcement and Dicarboxylic Acids Crosslinking Towards Polyvinyl Alcohol Properties. *Journal of Polymer Science Part A: Polymer Chemistry* **2016,** *54,* 2515-2525.

38. Biyani, M. V.; Weder, C.; Foster, E. J. Photoswitchable Nanocomposites Made from Coumarin-Functionalized Cellulose Nanocrystals. *Polymer Chemistry* **2014,** *5*, 5501-5508.

39. Camarero Espinosa, S.; Kuhnt, T.; Foster, E. J.; Weder, C. Isolation of Thermally Stable Cellulose Nanocrystals by Phosphoric Acid Hydrolysis. *Biomacromolecules* **2013,** *14*, 1223-1230.

40. Mueller, S.; Weder, C.; Foster, E. J. Isolation of Cellulose Nanocrystals from Pseudostems of Banana Plants. *RSC Advances* **2014,** *4*, 907-915.

41. Schroers, M.; Kokil, A.; Weder, C. Solid Polymer Electrolytes Based on Nanocomposites of Ethylene Oxide–Epichlorohydrin Copolymers and Cellulose Whiskers. *Journal of Applied Polymer Science* **2004,** *93*, 2883-2888.

42. Capadona, J. R.; Shanmuganathan, K.; Tyler, D. J.; Rowan, S. J.; Weder, C. Stimuli-Responsive Polymer Nanocomposites Inspired by the Sea Cucumber Dermis. *Science* **2008,** *319*, 1370.

43. Sapkota, J.; Kumar, S.; Weder, C.; Foster, E. J. Influence of Processing Conditions on Properties of Poly (Vinyl Acetate)/Cellulose Nanocrystal Nanocomposites. *Macromolecular Materials and Engineering* **2015,** *300*, 562-571.

44. Sapkota, J.; Shirole, A.; Foster, E. J.; Martinez-Garcia, J. C.; Lattuada, M.; Weder, C. Polymer Nanocomposites with Nanorods Having Different Length Distributions. *Polymer,* **2017,** *110,* 284-291.

45. Kaczmarek, H.; Kamińska, A.; Kowalonek, J.; Szalla, A. Changes of Poly(Ethylene Oxide) Photostability by Doping with Nickel(Ii) Chloride. *Journal of Photochemistry and Photobiology A: Chemistry* **1999,** *128*, 121-127.

46. Shirole, A.; Sapkota, J.; Foster, E. J.; Weder, C. Shape Memory Composites Based on Electrospun Poly(Vinyl Alcohol) Fibers and a Thermoplastic Polyether Block Amide Elastomer. *ACS Applied Materials & Interfaces* **2016,** *8*, 6701-6708.

47. Endes, C.; Mueller, S.; Kinnear, C.; Vanhecke, D.; Foster, E. J.; Petri-Fink, A.; Weder, C.; Clift, M. J. D.; Rothen-Rutishauser, B. Fate of Cellulose Nanocrystal Aerosols Deposited on the Lung Cell Surface in Vitro. *Biomacromolecules* **2015,** *16*, 1267-1275.

48. Van Munster, E. B.; Kremers, G. J.; Adjobo-Hermans, M. J. W.; Gadella, T. W. J. Fluorescence Resonance Energy Transfer (Fret) Measurement by Gradual Acceptor Photobleaching. *Journal of Microscopy* **2005,** *218*, 253-262.

49. Ridler, T. W.; Calvard, S. Picture Thresholding Using an Iterative Selection Method. *IEEE trans syst Man Cybern* **1978,** *8*, 630-632.

50. Schneider, C. A.; Rasband, W. S.; Eliceiri, K. W. Nih Image to Imagej: 25 Years of Image Analysis. *Nat Meth* **2012,** *9*, 671-675.

51. Mendez, J.; Annamalai, P. K.; Eichhorn, S. J.; Rusli, R.; Rowan, S. J.; Foster, E. J.; Weder, C. Bioinspired Mechanically Adaptive Polymer Nanocomposites with Water-Activated Shape-Memory Effect. *Macromolecules* **2011,** *44*, 6827-6835.

52. Nicharat, A.; Sapkota, J.; Weder, C.; Foster, E. J. Melt Processing of Polyamide 12 and Cellulose Nanocrystals Nanocomposites. *Journal of Applied Polymer Science* **2015,** *132*, doi:10.1002/app.42752.

53. Favier, V.; Chanzy, H.; Cavaille, J. Y. Polymer Nanocomposites Reinforced by Cellulose Whiskers. *Macromolecules* **1995,** *28*, 6365-6367.

54. Yegneswaran, S.; Wood, G. M.; Esmon, C. T.; Johnson, A. E. Protein S Alters the Active Site Location of Activated Protein C above the Membrane Surface: A Fluorescence Resonance Energy Transfer Study of Topography. *Journal of Biological Chemistry* **1997,** *272*, 25013-25021.

55. Zammarano, M.; Maupin, P. H.; Sung, L.-P.; Gilman, J. W.; McCarthy, E. D.; Kim, Y. S.; Fox, D. M. Revealing the Interface in Polymer Nanocomposites. *ACS Nano* **2011,** *5*, 3391-3399.

56. Kinoshita, A.; Whelan, C. M.; Smith, C. J.; Mikhailenko, I.; Rebeck, W. G.; Strickland, D. K.; Hyman, B. T. Demonstration by Fluorescence Resonance Energy Transfer of Two Sites of Interaction between the Low-Density Lipoprotein Receptor-Related Protein and the Amyloid Precursor Protein: Role of the Intracellular Adapter Protein Fe65. *Journal of Neuroscience* **2001,** *21*, 8354-8361.

57. Kunida, K.; Matsuda, M.; Aoki, K. Fret Imaging and Statistical Signal Processing Reveal Positive and Negative Feedback Loops Regulating the Morphology of Randomly Migrating Ht-1080 Cells. *Journal of Cell Science* **2012**.

58. Lossi, L.; Cocito, C.; Alasia, S.; Merighi, A. Ex Vivo Imaging of Active Caspase 3 by a Fret-Based Molecular Probe Demonstrates the Cellular Dynamics and Localization of the Protease in Cerebellar Granule Cells and Its Regulation by the Apoptosis-Inhibiting Protein Survivin. *Molecular Neurodegeneration* **2016,** *11*, 1-20.

59. Gordon, G. W.; Berry, G.; Liang, X. H.; Levine, B.; Herman, B. Quantitative Fluorescence Resonance Energy Transfer Measurements Using Fluorescence Microscopy. *Biophysical Journal* **1998,** *74*, 2702-2713.

TOC Figure

A Simple and Versatile Strategy to Improve the Mechanical Properties of Polymer Nanocomposites with Cellulose Nanocrystals

Worarin Meesorn, Anuja Shirole, Dimitri Vanhecke, Lucas Montero de Espinosa, and Christoph Weder